Optimization of the Process Parameters for Micro-Milling Thin-Walled Micro Parts Using Advanced Algorithms

Peng Wang
Harbin Institute of Technology https://orcid.org/0000-0002-2653-5367
Qingshun Bai (Qshbai@hit.edu.cn)
Harbin Institute of Technology
Kai Cheng
Brunel University London
Liang Zhao
Harbin Institute of Technology
Hui Ding
Harbin Institute of Technology

Research Article

Keywords: thin-walled microscale parts, micro-milling, fractal dimension, principal component analysis, advanced optimization algorithms

Posted Date: January 7th, 2022

DOI: https://doi.org/10.21203/rs.3.rs-1227258/v1

Optimization of the process parameters for micro-milling thin-walled micro parts using advanced algorithms

Peng Wang[1], Qingshun Bai[1*], Kai Cheng[2], Liang Zhao[1], Hui Ding[1]

[1]*School of Mechanical and Electrical Engineering, Harbin Institute of Technology, Harbin 150001, China*

[2]*Department of Mechanical and Aerospace Engineering, Brunel University London, Uxbridge UB8 3PH, UK*

**Corresponding author: Qshbai@hit.edu.cn*

Abstract

The surface integrity and machining accuracy of thin-walled micro parts are significantly affected by micro-milling parameters mostly because of their weak stiffness. Furthermore, there is still a lack of studies focusing on parameters optimization for the fabrication of thin-walled microscale parts. In this paper, an innovative approach is proposed for the optimization of machining parameters with the objectives of surface quality and dimension accuracy, which integrates the Taguchi method, principal component analysis method (PCA) and the Non-dominated sorting genetic algorithm (NSGA-II). In the study, surface arithmetic average height S_a, surface root mean square height S_q, and 3-D fractal dimension D_s are selected to evaluate surface quality. Then micro-milling experiments are conducted based on the Taguchi method. According to the experimental results, the significance of machining parameters can be determined by range analysis. Besides, regression models for the responses are developed comparatively, and the PCA method is employed for dimension reduction of the optimization objective space. Finally, two combinations of machining parameters with the highest satisfaction are obtained through NSGA-II, and verification experiments are carried out. The results show that the surface quality and dimension accuracy of the thin-walled microscale parts can be simultaneously improved by using the proposed approach.

Keywords: thin-walled microscale parts; micro-milling; fractal dimension; principal component analysis; advanced optimization algorithms.

1. Introduction

Usually, the microscale is defined as 1μm-1000μm in the field of mechanical processing [1]. Thin-walled microscale parts refer to the component structures with characteristics of microscale size and a height-to-thickness ratio greater than 5. Thin-walled microscale parts are increasingly in demand in many fields, including microelectrodes, microfluidic devices, micro/miniature dies and moulds [2, 3]. Micro-milling has the advantages of high production efficiency and high processing accuracy. Therefore, it is increasingly used in the processing of thin-walled microscale parts. However, both the thin-walled microscale part and micro-milling tools have weak stiffness, which brings challenges for its fabrication, especially for difficult-to-machine materials like Ti-6Al-4V alloy [4]. So, it is necessary to further investigate the machining process of thin-walled microscale parts.

Low surface quality and dimensional error are common problems in the processing of thin-walled microscale parts. An effective way to address these problems is to investigate the effects of machining parameters on processing quality and obtain the optimal parameters using an appropriate optimization method. Based on finite element analysis and response surface method (RSM) experiments, the effects of machining parameters were analyzed, and spindle speed and radial depth of cut were found as the most important factors for the burr height in micro-milling of thin-walled structure [5]. In thin wall fabrication, the effect of the axial depth of cut on the surface quality was found nonlinear [6]. Previous research showed that the interaction of radial cutting depth and axial cutting depth significantly influences surface roughness [7]. However, Kant [8] pointed out the feed per tooth is the most important machining parameter to reduce surface roughness and power consumption, followed by the depth of cut and cutting speed. To characterize the surface quality comprehensively, the fractal dimension method is employed. It was found that the fractal dimension measured by the mechanical method and the optical method can characterize the surface topography well, and it had a good correlation with the roughness value [9]. The surface of thin-walled microscale parts analyzed by three-dimensional fractal dimension D_s had better results than the surface roughness S_a and S_q [10].

Many researchers have endeavored to obtain optimal machining parameters. For improving machining quality, an optimization procedure based on the genetic algorithm and neural network was proposed to minimize surface roughness [11]. A method for simultaneous optimization of the burr width and surface roughness was also proposed using Taguchi-based grey correlation analysis [12]. Sahu and Ballav [13] performed optimization balancing surface roughness and cutting force of the turning process. Artificial neural network and particle swarm algorithm were used for optimizing

cutting force and surface roughness at the same time, and verification tests were carried out. The results showed that both the cutting force and surface quality were improved significantly [14]. For machining efficiency and cost, a method integrated Taguchi method, response surface method and multi-objective particle swarm optimization algorithm was present for the objectives of specific energy consumption and processing time [15]. The machining parameters of the multi-pass turning operation were optimized by the genetic algorithm. The constraints of the model include tool life, cutting power consumption and cutting force. This method generated lower unit production costs compared with the previous results from the literature [16]. Cutting energy and material removal rate were optimized based on Taguchi's experimental design and signal-to-noise ratio [17]. The optimal parameters combination was determined for the minimum unit production cost through the colony algorithm [18]. In multi-objective optimization problems, different objectives are conflicting in nature. Optimizing one of the objectives may cause the deterioration of the others, and multi-objective optimization methods are easily trapped in local optimal solutions. NSGA-II is widely used for its good robustness and global search capabilities. Qu et al. [19] found that the NSGA-II has the best optimization performance in the multi-objective problem in the milling process of thin-walled structures. NSGA-II was used for minimizing the tool life and processing cost in the micro-milling process, and the obtained results were better than those in the previous literature [20]. For cutting Inconel 718, a method for the selection of optimal process parameters was proposed based on NSGA-II [21].

Due to the microscale size and low stiffness of thin-walled microscale parts, the errors of machine tools and cutting tools are more likely to be reflected on the workpiece, which makes the machining quality is more sensitive to the selection of machining parameters. However, most previous studies on the optimization of machining parameters focus on macroscale thin-walled parts. And fewer researches are performed with consideration of more than four objectives simultaneously in the micro-milling process. This paper firstly conducts orthogonal experiments for micro-milling thin-walled microscale parts. Then the effects of machining parameters on the optimization objectives are analyzed according to the obtained results. Besides, a method for the optimization of machining parameters using PCA-based NSGA-II is proposed. The optimal parameters for the best surface quality and dimension accuracy can be obtained through this method. Finally, micro-milling experiments are performed to verify the effectiveness of the proposed method.

2. Method and experiments

2.1 Procedure for the optimization of machining parameters

Fig. 1 depicts the flowchart of the machining parameters optimization for the thin-walled microscale parts. Dimensional error D_e, arithmetic average height S_a, root mean square height S_q, and surface fractal dimension D_s are considered simultaneously in this work. The thin-walled part shown in Fig. 2 is fabricated by dry micro-milling. The workpiece material is Ti-6Al-4V, and the values for b, h and l are 100 μm, 600 μm and 5 mm, respectively. Firstly, experiments based on the Taguchi method are carried out. The surface topographies and dimensions of the machined parts are measured by white light interferometer (WLI) and coaxial image instrument (CII), respectively. Then multiple regression models are developed based on stepwise regression. Besides, the PCA is performed for dimension reduction. After that, cutting parameters are optimized by NSGA-Ⅱ and the Pareto optimal solution set is obtained. Finally, two combinations of machining parameters with the highest satisfaction are selected for the verification experiments.

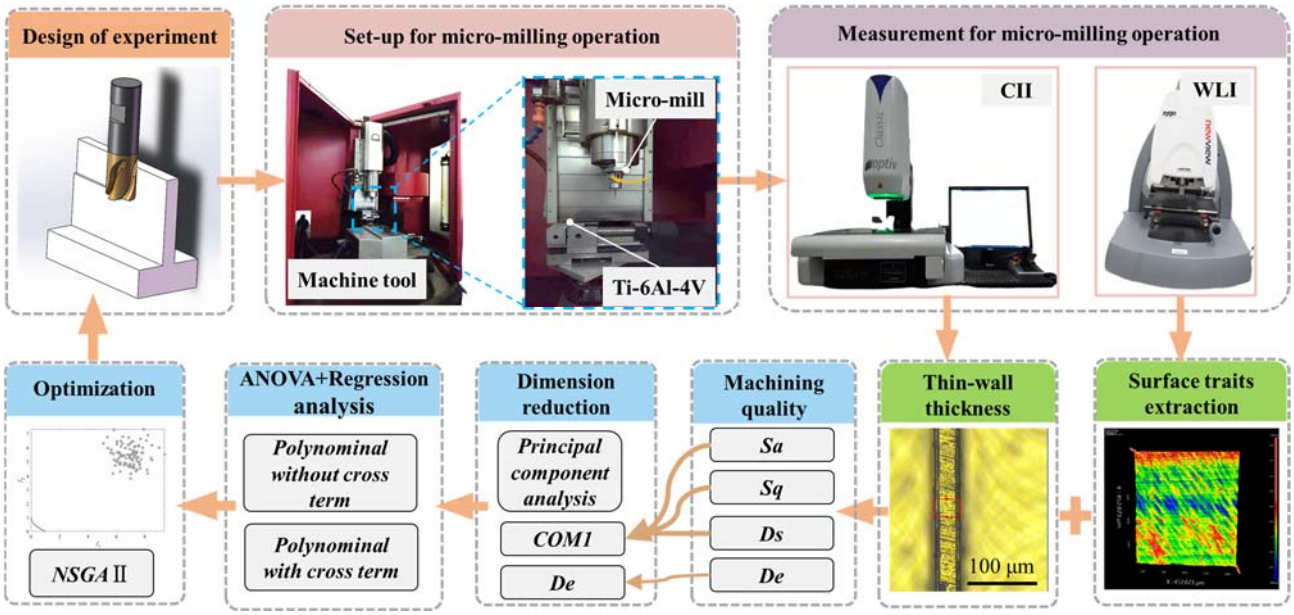

Fig. 1 Flow chart of machining parameters optimization

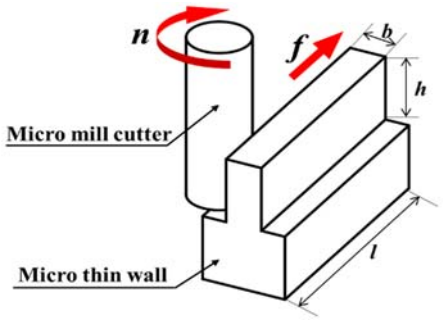

Fig. 2 The schematic of the micro-milling process

2.2. Optimization objectives

2.2.1 Surface roughness

The surface arithmetic average height S_a and the surface root mean square height S_q are selected to reflect the surface roughness. S_a represents the average geometric error of the milled surface and S_q represents the root mean square of the geometric error of the milled surface respectively. The calculation methods are shown as follows.

$$\begin{cases} S_a = \iint_S \left|\Phi(x,y) - \xi(x,y)\right| dxdy / S \\ S_q = \sqrt{\iint \Phi^2(x,y)\, dxdy / S} \end{cases} \tag{1}$$

Where $\Phi(x,y)$ denotes the height information of the surface, and $\xi(x,y)$ corresponds to the reference plane of the surface.

2.2.2 3-D surface fractal dimension

The characteristics of the machined surface cannot be fully present by surface roughness. Therefore, the 3-D fractal dimension D_s is employed to characterize the machined surface from the perspective of the surface structure. Among the 3-D fractal dimension calculation methods for the mechanical machining surface, the box-counting method has the best accuracy [22]. So, it is adopted as one of the key objectives of optimization. The box-counting method uses cubes with the same side length to segment the three-dimensional surface topography, and the minimum number of boxes covering the image surface is employed for calculating the fractal dimension. The fractal dimension can be expressed as Eq. (1).

$$D_s = \frac{\ln N(\varepsilon)}{\ln\left(\varepsilon^{-1}\right)} \tag{2}$$

Where ε represents the side length of the box, and $N(\varepsilon)$ represents the number of boxes.

2.2.3 Dimension error

The dimension error is the deviation between the actual dimension and the design dimension of the thin-walled structure in the thickness direction. As shown in Fig.3, deflection is inevitable due to the weak stiffness of the thin-walled micro part and micro-milling tool. The dimension error D_e can be expressed as.

$$D_e = \left|D_a - D_i\right| \tag{3}$$

Where D_a is the actual dimension, and D_i is the design dimension.

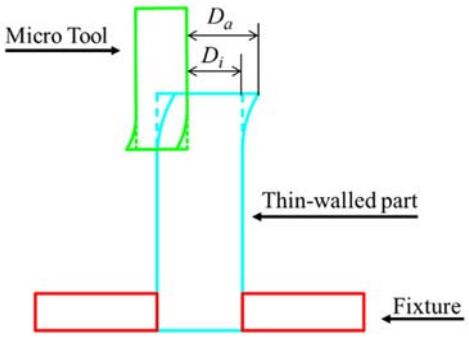

Fig. 3 The deflection of thin-walled micro part and micro-milling tool

2.3 Experimental design

As shown in Fig. 4, the micro-milling experiments are carried out on the KERN Evo five-axis vertical machining center. The cutting tool is a four-edged carbide end mill with a diameter of 1 mm and 45° helix angle, and the cutting strategy is dry milling. Tool wear has a significant influence on the machining process [23,24], in order to avoid the effects of tool wear on the machining results, a fresh tool is used in each experiment. The workpiece material is Ti-6Al-4V alloy.

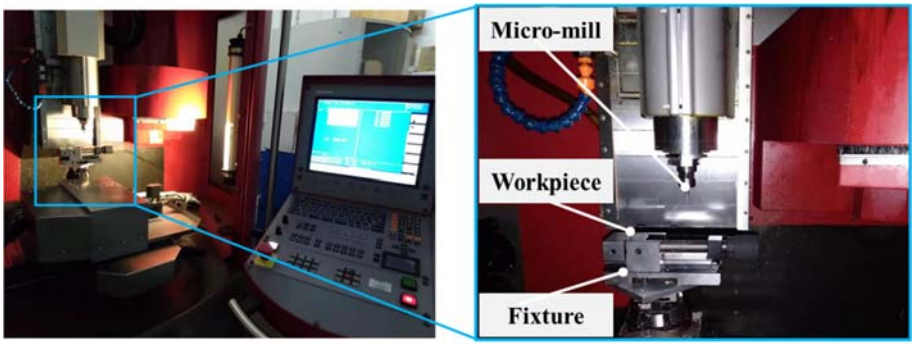

Fig. 4 Micro-milling system

In order to analyze the effects of machining parameters (spindle speed n, feed per tooth f_z, axial milling depth a_p, and radial milling depth a_e) on machining quality, an orthogonal experiment is designed, ignoring the interaction among all the parameters. The Taguchi experiment table L16 (4^4) is chosen for experiment design, and the process parameters and their levels are shown in Table 1.

Table 1 Machining parameters used in the experiment

Symbol	Process Parameters	Units	Level			
			1	2	3	4
A	Spindle speed (n)	r/min	15000	20000	25000	30000
B	Axial depth of cut(a_p)	μm	50	60	100	150
C	Radial depth of cut(a_e)	μm	20	30	40	50
D	Feed per tooth (f_z)	μm/tooth	0.5	1.5	2.5	3.5

2.4. Multi-objective optimization method using PCA-based NSGA-II

The non-dominated sorting genetic algorithm with elite strategy (NSGA-II) is a multi-objective evolutionary algorithm based on the non-inferior solution (Pareto) set. It has the characteristics of high optimization efficiency and good global searchability. Therefore, it has been widely used in the optimization of process parameters. But for the high-dimensional optimization objectives space with more than four functions, NSGA-II is incapable. Meanwhile, the visualization of results for high-dimensional objective space is rather difficult. So, the key step is to reduce the dimension of the 4-D optimization objectives space by means of principal component analysis (PCA).

3. Results and discussion

The results of the orthogonal experiments are shown in Table 2. When performing measurements, the results are averaged at three locations on the thin-walled parts.

Table 2 Results of the orthogonal experiments

No.	Symbol	Control factors				Responses			
		A	B	C	D	S_a(μm)	S_q(μm)	D_s	D_e(μm)
1	A1B1C1	15000	50	20	0.5	0.3153	0.4363	2.4534	1.4
2	A1B2C2	15000	60	30	1.5	0.4617	0.5600	2.4083	9.5
3	A1B3C3	15000	100	40	2.5	0.6920	0.9067	2.3982	4.6
4	A1B4C4	15000	150	50	3.5	0.3433	0.4420	2.4174	3.3
5	A2B1C2	20000	50	30	2.5	0.4087	0.5157	2.4119	11.2
6	A2B2C1	20000	60	20	3.5	0.1120	0.1563	2.5037	3.9
7	A2B3C4	20000	100	50	0.5	0.2270	0.2867	2.5012	3.3
8	A2B4C3	20000	150	40	1.5	0.3217	0.3873	2.4509	4.2
9	A3B1C3	25000	50	40	3.5	0.3337	0.4477	2.4112	8.7
10	A3B2C4	25000	60	50	2.5	0.3873	0.5103	2.4070	4.1
11	A3B3C1	25000	100	20	1.5	0.3670	0.4717	2.4085	2.1
12	A3B4C2	25000	150	30	0.5	0.2327	0.3083	2.4762	0.1
13	A4B1C4	30000	50	50	1.5	1.3740	1.8307	2.3968	2.1
14	A4B2C3	30000	60	40	0.5	0.1823	0.2350	2.4557	8.4
15	A4B3C2	30000	100	30	3.5	0.4407	0.5537	2.4149	3.6
16	A4B4C1	30000	150	20	2.5	0.4987	0.6200	2.4100	11.5

3.1 Effects of machining parameters on surface roughness

Fig. 5 shows the variations of the three-dimensional roughness with machining parameters. The surface roughness decreases when the spindle speed increases from 15000 r/min to 20000 r/min. While, as the spindle speed exceeds 20000 r/min, the surface roughness shows an increasing trend. Generally, high spindle speed can lead to more heat generation, which can cause the thermal softening

effect on the Ti-6Al-4V material. However, the continuous spindle speed increase can cause rapid tool wear and enlarge cutting tooltips, which can change the material removal mechanism and deteriorate surface quality. The minimum surface roughness is found when the axial cutting depth is 60 μm. When the axial cutting depth is less than this chip thickness, the obvious ploughing and extrusion effect between the cutting edge and the workpiece can damage the surface quality. The surface roughness shows an increasing trend as the radial depth of cut increases. And a significant rise is observed when the radial depth of cut drops from 40 μm to 50 μm. In addition to the rise in cutting force, the stability of the tool-workpiece system goes down when the radial depth of cut increases, which can cause chatter and a significant deterioration of surface quality. The surface roughness reaches the largest value at 1.5 μm/tooth and it has a rapid decrease when the feed per tooth reaches 0.5 μm/tooth. The change in surface roughness presents an opposite trend compared to macro-scale milling when the feed per tooth increases from 1.5 μm/tooth to 3.5 μm/tooth. In Fig. 4, the change of S_q is greater than that of S_a, which means that S_q is more sensitive to the variations of machining parameters. And a combination of machining parameters for minimum surface roughness is obtained: n=20000 r/min, a_p= 60μm, a_e=20 μm, and f_z=0.5 μm/tooth.

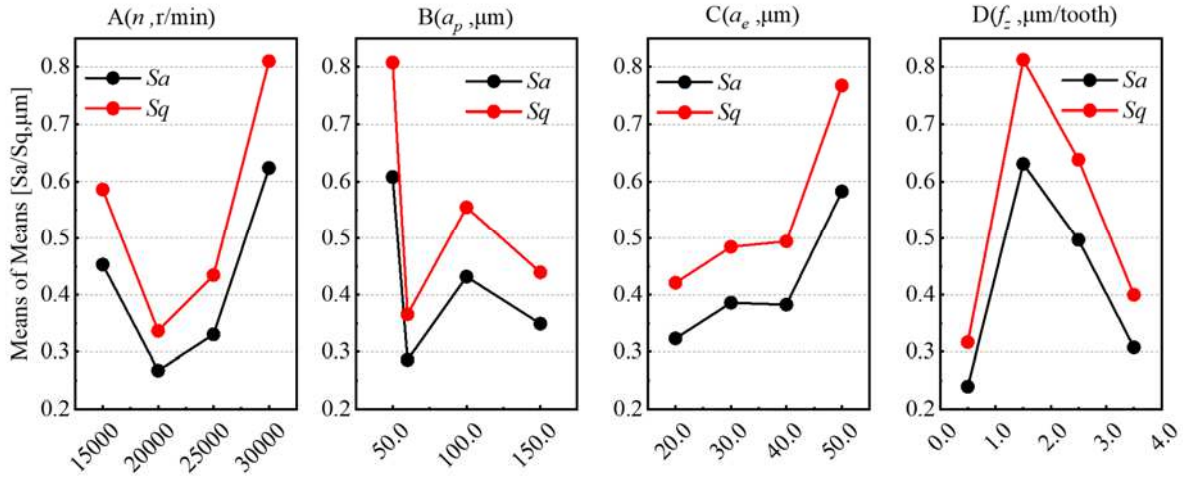

Fig. 5 Main effects plot for S_a & S_q

3.2 Effects of machining parameters on 3-D fractal dimension

In Fig. 6, the variations of surface fractal dimension D_s with machining parameters show an opposite trend with the surface roughness. In order to further discuss the relationship between the fractal dimension and surface roughness, the linear fit is performed between D_s and S_a. Fig.7 shows the correlation between D_s and S_a. An obvious negative correlation can be observed, which is consistent with the conclusions in previous literature [22]. Therefore, a good surface quality means a small surface roughness and a big fractal dimension value.

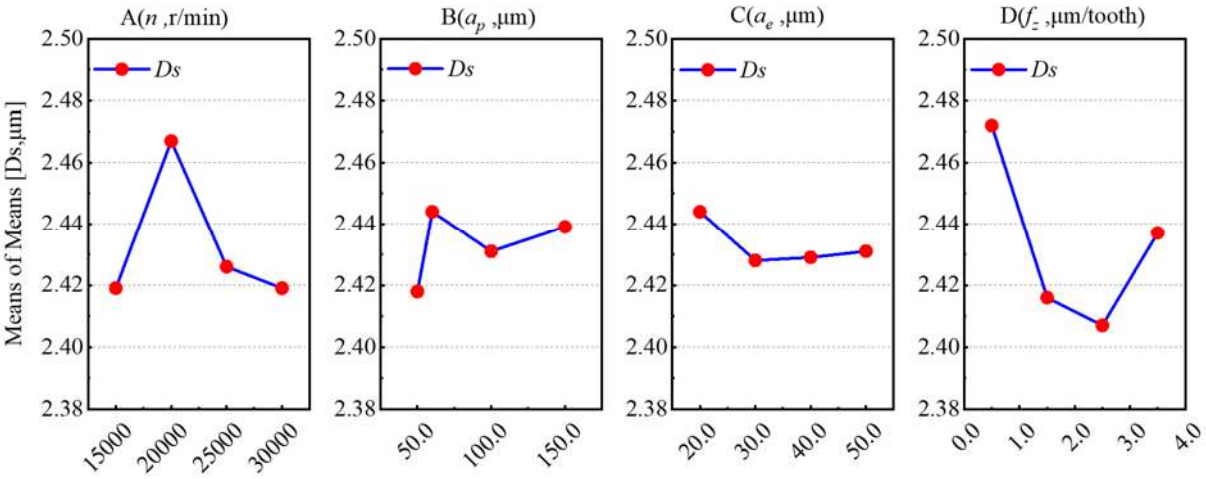

Fig. 6 Main effects plot for D_s

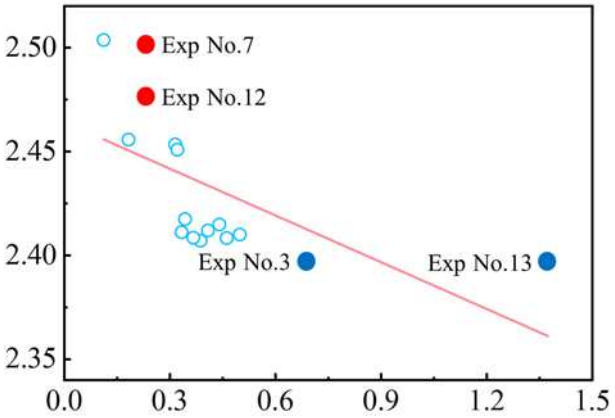

Fig. 7 Relation between S_a and D_s

However, the negative correlation between D_s and S_a is not a one-to-one correspondence. Fig. 8 shows four selected surface topographies in all the experimental results.

Comparing the surface topographies of the 7th and the 12th experiments, a conclusion can be drawn that when the surface roughness is close, the fractal dimension of the machined surface with defects is smaller. Surface topographies of the 3rd and the 13th experiments show that when the fractal dimension is close, the surface roughness may have an obvious difference. It can be seen, compared with the surface roughness, the surface fractal dimension is more sensitive to the defects of the machined surface. Therefore, the combination of surface roughness and surface fractal dimension has a better characterization performance.

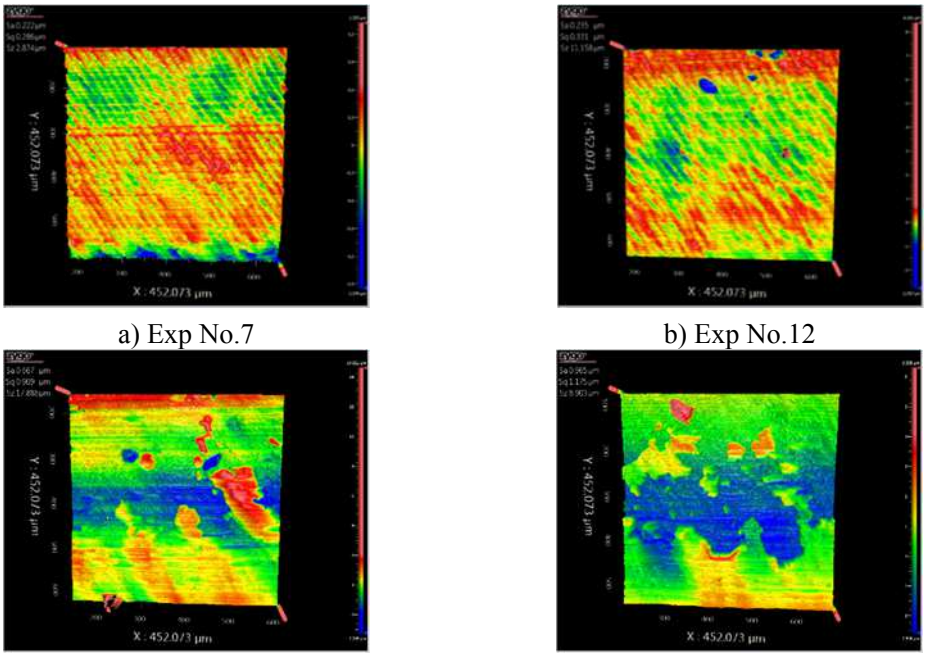

a) Exp No.7 b) Exp No.12

c) Exp No.3 d) Exp No.13

Fig. 8 3-D surface profiles obtained for selected cutting conditions

3.3 Effects of machining parameters on dimension deviation

Fig. 9 shows the effects of micro-milling parameters on the workpiece actual size. As can be seen, the actual size of the thin-walled parts is greater than 100 μm, except for one group of the results. This is caused by the deflection during the machining process due to the weak stiffness of the micro-milling cutter and the thin-walled structure.

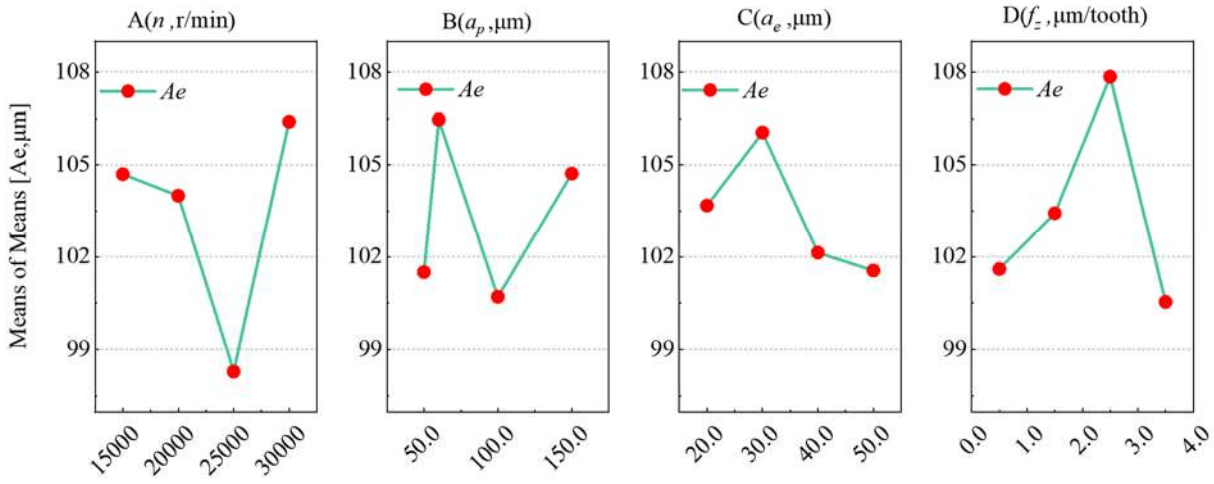

Fig. 9 Main effects plot for A_e

Fig. 10 shows the largest dimension error is at 30000 r/min. A larger spindle speed can cause rapid tool wear and increase the micro-milling force, which can enlarge the deflection of the thin-walled structure.

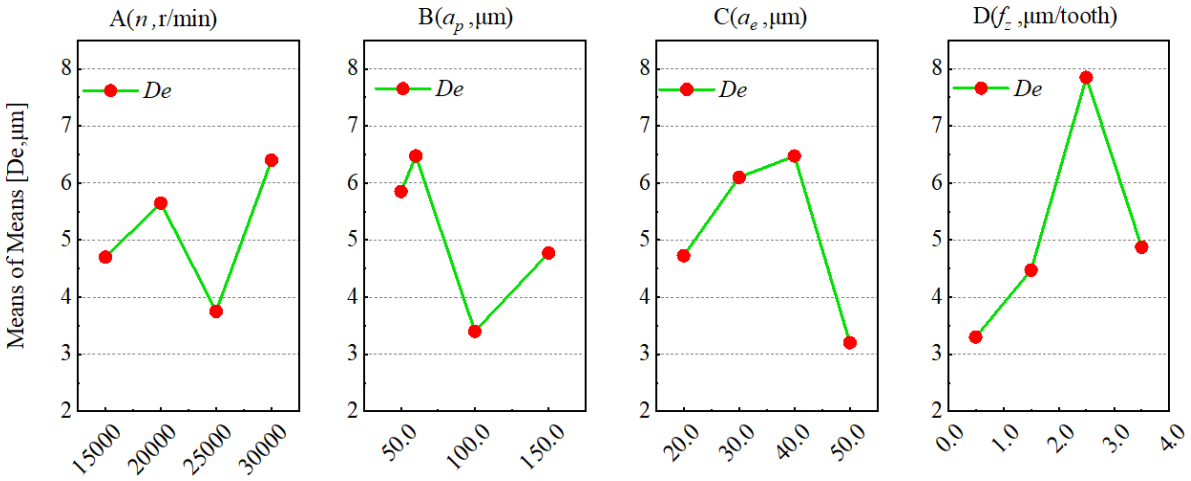

Fig. 10 Main effects plot for D_e

When the axial depth of cut is less than 60 μm, the ploughing and extrusion effects can lead to an increase in dimensional error. The radial depth of cut and the feed per tooth have similar effects on the dimension error. When the radial depth of cut reaches 50 μm and the feed per tooth reaches 3.5 μm/tooth, severe chip bending may produce a lot of heat. Then the temperature rise can lead to a thermal softening effect on the workpiece material. Therefore, the micro-milling force may decrease, so do the deflection and dimension errors. And a combination of machining parameters for minimum dimension error can be obtained as n=25000 r/min, a_p=100 μm, a_e=20 μm and f_z=0.5 μm/tooth.

3.4 Range analysis of optimization objectives

The significant contributions of the effects of machining parameters on the optimization objectives can be evaluated by range analysis value. Larger range values promise a more significant effect. And it can be calculated by Eq. (4).

$$R_j = \max(k_1, k_2, k_3, k_4) - \min(k_1, k_2, k_3, k_4) \quad (4)$$

Where k_i is the mean value of the i-th level of factor k, i =1, 2, 3, 4. R_j is the range value of the j-th factor. Table 3 shows that the significance of machining parameters is $R_{fz} > R_n > R_{ap} > R_{ae}$ for S_a, S_q, and D_s. But for D_e, there is $R_{fz} > R_{ae} > R_{ap} > R_n$. The effects of the parameters are different from results in previous studies [25,26].

Table 3 Range Analysis the results of orthogonal experiments

R_j	n	a_p	a_e	f_z
S_a	0.3556	0.3221	0.2596	0.3918
S_q	0.4734	0.4422	0.3464	0.4958
D_s	0.048	0.025	0.016	0.065
D_e	2.650	3.075	3.275	4.550

3.5 Multiple regression analysis

Polynomial regression has the advantages of simplicity, intuition, and low computational cost among many linear regression methods. Therefore, we choose the polynomial regression method to perform the regression analysis for the four optimization objectives. Meanwhile, a comparison is made between the quadratic fitting model using stepwise regression analysis and the model considering all the quadratic terms. The fitting performance of the model is evaluated by the significance of p value, adjusting coefficient of determination R^2 (adj), and Bayesian Information Criterion (BIC). The comparison results are shown in Fig. 11. For S_a, S_q, and D_e, the stepwise regression model has a smaller p value, i.e., better significance, and a smaller BIC value, i.e., avoiding overfitting. For D_s, the regression model with all quadratic terms has a larger R^2(adj), but the R^2(adj) of the stepwise regression model is also more than 90%.

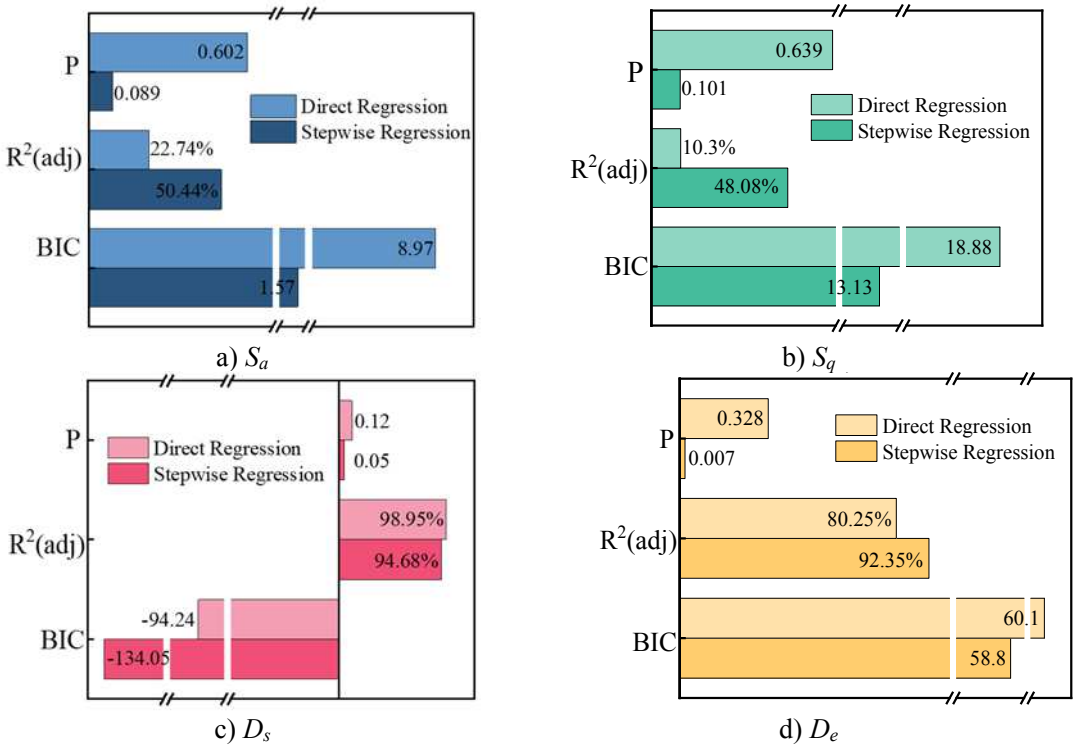

Fig. 11 Significance, adjusting R^2 and BIC criterion of regressions

From the analysis above, the complexity of the regression model does not guarantee good fitting performance. Therefore, the stepwise regression method is used in our work. The regression models are Eqs. (5)-(8):

$$S_a = (0.502353) - (1.37188e-4 \times A) + (0.0162087 \times B) + (0.0143241 \times C) - (0.175385 \times D) + (2.769e-9 \times A^2) - (7.20443e-5 \times B^2) - (0.00436369 \times C \times D) + (0.06038894 \times D^2) + (2.88859e-7 \times A \times B); \quad (5)$$

$$S_q = (1.36988) - (2.02668e-4 \times A) + (0.0205306 \times B) + (0.00441294 \times C) - (0.388259 \times D) + (4.2489e-9 \times A^2) - (9.01551e-5 \times B^2) + (0.0773889 \times D^2) + (3.3833e-7 \times A \times B); \quad (6)$$

$$D_s = (1.36988) - (2.02668e-4 \times A) + (0.0205306 \times B) + (0.00441294 \times C) - (0.388259 \times D) + (4.2489e-9 \times A^2) - (9.01551e-5 \times B^2) + (0.0773889 \times D^2) + (3.3833e-7 \times A \times B); \quad (7)$$

$$D_e = (-9.79754) - (0.000217969 \times A) + (0.243496 \times B) - (0.147253 \times C) + (1.56598 \times D) - (0.000786049 \times B^2) + (0.00000984933 \times A \times C) - (0.0000988167 \times A \times D); \quad (8)$$

Fig. 12 shows the consistency evaluation between the calculation results of regression models and the experimental results. The results show that the regression models present a good predictive ability.

3.6 Dimension reduction analysis of optimization objectives

Fig. 13 is the correlation matrix of optimization objectives. The correlation coefficient between the dimension error D_e and the surface roughness S_a is only 0.292, and the correlation between the dimension error and other optimization objectives is also very low. Therefore, the dimension error can be considered as an independent optimization objective.

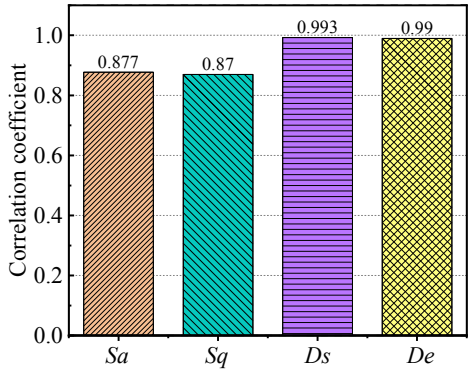

Fig. 12 Pearson correlations

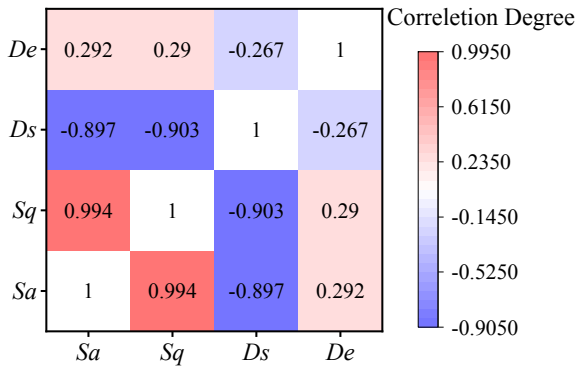

Fig. 13 Relation matrix of the objective function

Table 4 shows the KMO and Bartlett test results of principal component analysis. The Kaiser-Meyer-Olkin measurement value is 0.564, which is greater than 0.5.

Table 4 KMO and Bartlett's test

Sampling adequacy	Bartlett's test of sphericity		
KMO measure	Approximate chi-square	df	Sig.
0.564	86.194	3	0.000

That means PCA analysis for S_a, S_q, and D_s has a good dimension reduction effect. The p value of Bartlett's test is less than 0.01, which proves that the optimization objectives have a good linear relationship. Therefore, PCA analysis can be employed to perform dimension reduction analysis on the selected optimization objectives. Fig. 14 shows the common factor variance in PCA analysis.

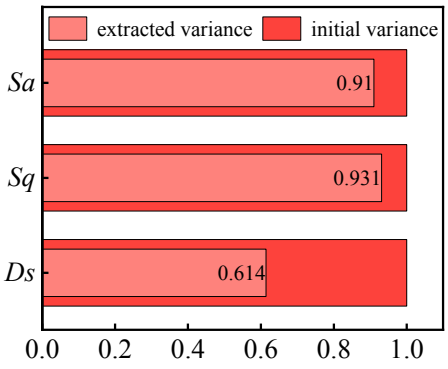

Fig. 14 Common factor variance

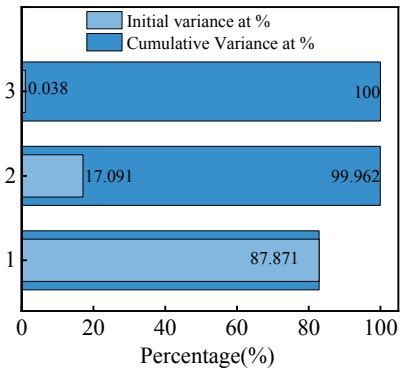

Fig. 15 Explained total variance

Unlike the initial variation, all the explanation degree of surface characteristics variables is less than 100%. The variation of fractal dimension can be explained only by 61.4%. Fig. 15 is the total explained variance of the PCA analysis. The analysis results show that the first principal component contains the most surface characteristics variation data, accounting for 87.871% of the total accumulation. Combining with the analysis results in Fig. 16, only one principal component has an eigenvalue greater than 1. Therefore, only one principal component needs to be retained.

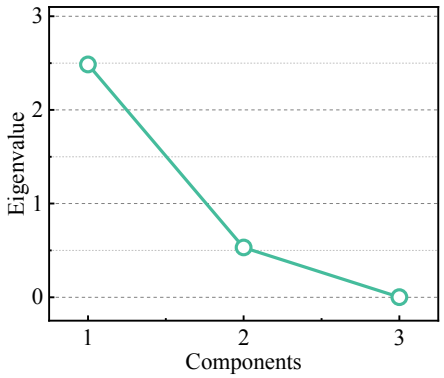

Fig. 16 Scree plot

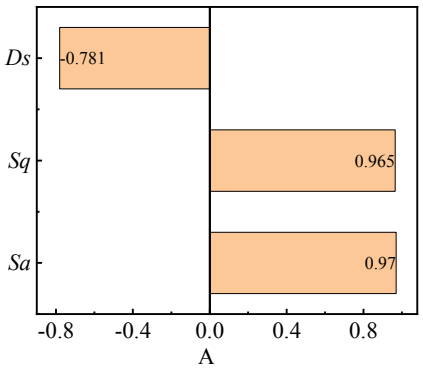

Fig. 17 Component matrix

Fig. 17 details the component matrix, which represents the factor loading matrix A in the PCA analysis. The transformation matrix in PCA analysis can be obtained by the principal component

loading matrix U and the factor loading matrix A. The relationship is shown as follows:

$$U_i = A_i / \sqrt{\lambda_i} \tag{9}$$

Where λ_i is the eigenvalue. Only one principal component is extracted, so, i =1. According to Eq. (9), the principal component PC_1 is:

$$PC_1 = 0.970SA + 0.965SQ - 0.781DS \tag{10}$$

Where SA, SQ, and DS are the standard scores of the original optimization objectives after standardization. The relationship between the standardization process and the original optimization objective is:

$$X'_{mn} = \left(X_{mn} - \bar{X}_m\right) / \sigma_m \tag{11}$$

Where X'_{mn} represents the n-th sample of the m-th objective after normalization, and X_{mn} represents the n-th sample of the m-th original objective. And the remaining variable formulas are:

$$\bar{X}_m = \sum_{n=1}^{p} X_{mn} / p \tag{12}$$

$$\sigma_m = \sqrt{\sum_{n=1}^{p}\left(X_{mn} - \bar{X}_m\right)^2 / p} \tag{13}$$

Where p is the total number of samples. The calculated mean value matrix and standard deviation matrix are:

$$\bar{X}_m = \begin{bmatrix} 0.4186 \\ 0.5418 \\ 2.4328 \end{bmatrix} \tag{14}$$

$$\sigma_m = \begin{bmatrix} 0.2891 \\ 0.385 \\ 0.0358 \end{bmatrix} \tag{15}$$

Then the principal component PC_1 can be expressed as:

$$PC_1 = 4.108S_a + 3.2975S_q + 29.6657D_s^{-1} - 16.8614 \tag{16}$$

3.7 Multi-objective optimization results

In the calculation, multi-objective optimization for the smallest roughness, the largest surface fractal dimension, and the smallest dimension error is carried out. According to the constructed constraint equation and the value range of each machining parameter, the optimal combinations of machining parameters can be obtained. On the basis of the analysis in section 3.6, optimization objective functions after dimension reduction can be expressed as:

$$\min f_i(X) = \begin{bmatrix} f_1(X) = PC_1 \\ f_2(X) = D_e \end{bmatrix} \tag{17}$$

The decision variable is $X = [n\ a_p\ a_e\ f_z]^{\mathrm{T}}$. And the range of their constraints is 20 μm≤a_e≤50 μm, 50 μm≤a_p≤150 μm, 15000 μm≤n≤30000 μm, 0.5 μm/tooth≤f_z≤3.5 μm/tooth.

NSGA-II is employed for the optimization of machining parameters. The initial population number is set as 500, and the evolutionary generation is 1500. The Pareto front and the Pareto optimal solution set are obtained, as shown in Fig. 18.

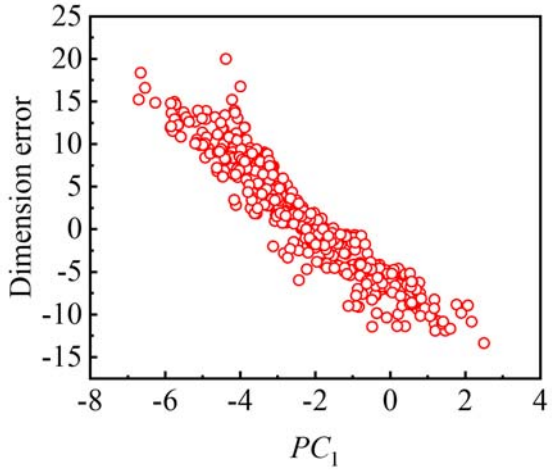

Fig. 18 Pareto front of optimized results

A function evaluating the membership degree is proposed for the selection of machining parameters in the Pareto solution set, as shown in Eq. (18).

$$p_i = \frac{f_{i\max} - f_i}{f_{i\max} - f_{i\min}} \tag{18}$$

Where f_{imax} and f_{imin} are the maximum and minimum value of the i-th objective function, respectively, and f_i is the value of the i-th objective function.

The standardized satisfaction degree of each solution in the Pareto optimal solution set can be obtained from Eq. (19).

$$P_i = \frac{1}{N}\sum_{i=1}^{N} p_i \tag{19}$$

The parameters with the top two largest P values in the Pareto optimal solution set are selected.

$$\begin{aligned} X_1 &= [27880, 115, 50, 0.525] \\ X_2 &= [24230, 131, 50, 1.180] \end{aligned} \tag{20}$$

3.8 Optimization results verification

In order to verify the effectiveness of the solutions obtained in the multi-objective optimization,

comparison experiments are carried out. The optimal combinations of machining parameters and the combinations of machining parameters for the best surface quality and minimum dimension error in previous single factor experiments are also selected for the comparison. The levels of machining parameters are shown in Table 5, in which Case 1 and Case 2 are the optimal results and Case 3 and Case 4 indicate the parameters obtained in single factor experiments

Table 5 Machining parameters of the validation experiments

Symbol	Case 1	Case 2	Case 3	Case 4
	Optimal	Optimal	S_a (S_q) Min./D_s Max.	D_e Min.
A	27880	24230	20000	25000
B	115	131	60	100
C	50	50	20	50
D	0.525	1.18	0.5	0.5

The actual size of the workpiece is measured by the coaxial image instrument and 3-D topography is measured by the white light interferometer after conducting experiments. The results are shown in Fig. 19 and Fig. 20, respectively.

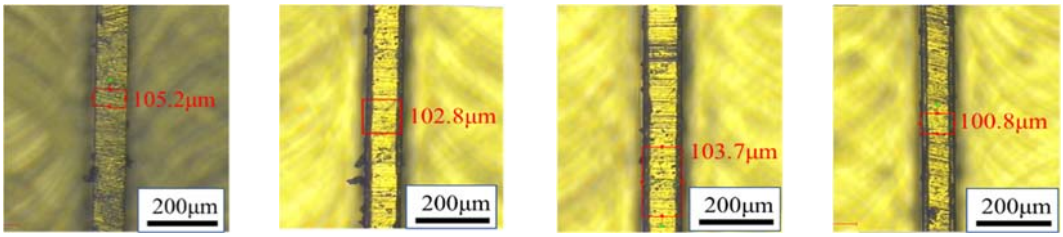

a) Case 1 b) Case 2 c) Case 3 d) Case 4

Fig. 19 Dimensions of the thin-walled micro parts

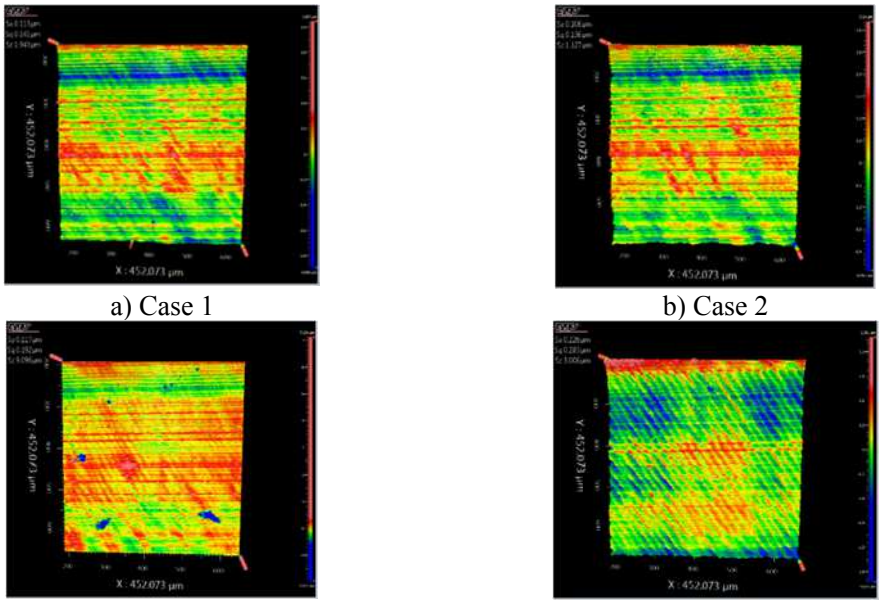

a) Case 1 b) Case 2

c) Case 3 d) Case 4

Fig. 20 Surface topographies of the thin-walled micro parts

Table 6 lists the results of validation experiments. The surface roughness and surface fractal dimension of Case 2 are only inferior to the results of Case 3, and the dimension error of Case 2 is only inferior to the results of Case 4. So, the rationality and effectiveness of the proposed machining parameters optimization method are proved by the results of the validation experiment.

Table 6 Results of validation experiments

Symbol	Case 1	Case 2	Case 3	Case 4
	Optimal	Optimal	S_a(S_q)Min./D_s Max.	D_e Min.
S_a	0.117	0.113	0.106	0.226
S_q	0.192	0.141	0.136	0.283
D_s	2.4886	2.5032	2.5086	2.4406
D_e	3.7	2.8	5.2	0.8

4. Conclusions

This paper provides a strategy for the determination of optimal parameters in micro-milling thin-walled microscale parts using PCA-based NSGA-II. The dimension error D_e, the arithmetic average height S_a, the root mean square height S_q, and the surface fractal dimension D_s are considered as optimization objectives simultaneously. The combinations of optimal machining parameters can be acquired by this method. Finally, the optimized machining parameters are verified by micro-milling experiments.

(1) The significance contributions of machining parameters for S_a, S_q, and D_s are $R_{fz} > R_n > R_{ap} > R_{ae}$ by order and the significance contributions for D_e are $R_{fz} > R_{ae} > R_{ap} > R_n$ by order.

(2) The surface fractal dimension D_s and the arithmetic average height S_a show a negative correlation. And D_s is more sensitive to surface defects than S_a, according to the results of orthogonal experiments.

(3) Regression models of stepwise regression analysis have a good performance on fitting S_a, S_q, D_s, and D_e for its better significance, smaller BIC values, and bigger adjusting coefficient of determination compared with regression models with all the quadratic terms.

(4) The verification experiment results prove that the proposed method is effective, which can obtain optimal parameters for high surface quality as well as dimension accuracy in the micro-milling of thin-walled microscale parts.

Author contribution: Peng Wang: Conceptualization, methodology, writing-original draft. Qingshun Bai: Funding acquisition, supervision, formal analysis, writing-review and editing. Kai Cheng: supervision, formal analysis, writing-review and editing. Liang Zhao: validation, investigation, and equipment. Hui Ding: validation.

Funding: This research work was supported by the National Natural Science Foundation of China (Grant No. 52075129).

Data availability: The datasets used or analyzed during the current study are available from the corresponding author on reasonable request.

Code availability: This paper uses proprietary software and will be not available.

Declarations

Ethics approval: This work has no research involving human participants and/or animals.

Consent to participate: Not applicable.

Consent for publication: Not applicable.

Competing interests: No conflict of interest exists in the submission of this manuscript, and the manuscript is approved by all authors for publication.

References

[1] Cheng K., Huo D. (2013) Micro Cutting: Fundamentals and Applications. John Wiley & Sons.

[2] Lazoglu I., Mamedov A. (2016) Deformation of thin parts in micromilling. CIRP Annals 65(1):117-120. https://doi.org/10.1016/j.cirp.2016.04.077.

[3] Zhang G., Li W., Zhang Y., et al. (2020) Analysis and reduction of process energy consumption and thermal deformation in a micro-structure wire electrode electric discharge machining thin-wall component. Journal of Cleaner Production 244: 118763. https://doi.org/10.1016/j.jclepro. 2019.118763.

[4] Bai J., Bai Q., Tong Z., et al. (2018) Theoretical model for subsurface microstructure prediction in micro-machining Ti-6Al-4V alloy-experimental validation. International Journal of Mechanical Sciences 148: 64-72. https://doi.org/10.1016/j.ijmecsci.2018.08.014.

[5] Gao X., Cheng X., Ling S., et al. (2022) Research on optimization of micro-milling process for curved thin wall structure. Precision Engineering 73: 296-312. https://doi.org/10.1016/ j.precisioneng. 2021.09.015.

[6] Llanos I., Agirre A., Urreta H., et al. (2014) Micromilling high aspect ratio features using tungsten carbide tools. Proc IMechE Part B: J Engineering Manufacture 228(11): 1350-1358. https://doi.org/10.1177/ 0954405414522214.

[7] Ribeiro J. E., César M. B., Lopes H. (2017) Optimization of machining parameters to improve the surface quality. Procedia Structural Integrity 5:355-362. https://doi.org/10.1016/j.prostr. 2017.07.182.

[8] Kant G., Sangwan K.S. (2014) Prediction and optimization of machining parameters for minimizing power consumption and surface roughness in machining. Journal of Cleaner Production 83:151-164. https://doi.org/10.1016/j.jclepro.2014.07.073.

[9] Poljacek S. M., Risovic D., Furic K., et al. (2008) Comparison of fractal and profilometric methods for surface topography characterization. Applied Surface Science 254(11):3449-3458. https://doi.org/10.1016/j.apsusc.2007.11.040.

[10] Qu D., Wang B., Peng Z. (2017) The influence of processing parameters on surface characteristics in micro-milling thin-walled slot on elgiloy. Int J Adv Manuf Technol 92: 2843–2852. https://doi.org/10.1007/s00170-017-0298-x.

[11] Oktem H., Erzurumlu T., Erzincanli F. (2006) Prediction of minimum surface roughness in end milling mold parts using neural network and genetic algorithm. Materials & Design 27(9):735-

744. https://doi.org/10.1016/j.matdes.2005.01.010.

[12] Aslantas K., Ekici E., Çiçek A. (2018) Optimization of process parameters for micro milling of Ti-6Al-4V alloy using Taguchi-based gray relational analysis. Measurement 128:419-427. https://doi.org/10.1016/j.measurement.2018.06.066.

[13] Sahu K. K., Ballav R. (2017) Optimization of machining parameters of Aluminum-based hybrid composites using Gray Relation Analysis. Materials Today Proceedings 4(9):9977-9981. https://doi.org/10.1016/j.matpr.2017.06.305.

[14] Gopan V., Leo D., Evangeline G., et al. (2020) Experimental investigation for the multi-objective optimization of machining parameters on AISI D2 steel using particle swarm optimization coupled with artificial neural network. Journal of Advanced Manufacturing Systems 19(3):589-606. https://doi.org/10.1142/S0219686720500286.

[15] Li C., Xiao Q., Tang Y., et al. (2016) A method integrating Taguchi, RSM and MOPSO to CNC machining parameters optimization for energy saving. Journal of Cleaner Production 135:263-275. https://doi.org/10.1016/j.jclepro.2016.06.097.

[16] Yusup N., Zain A.M., Hashim S.Z.M. (2012) Evolutionary techniques in optimizing machining parameters: Review and recent applications (2007-2011). Expert Systems with Applications 39(10):9909-9927. https://doi.org/10.1016/j.eswa.2012.02.109.

[17] Mia M., Dey P.R., Hossain M.S., et al. (2018) Taguchi S/N based optimization of machining parameters for surface roughness, tool wear and material removal rate in hard turning under MQL cutting condition. Measurement 122:380-391. https://doi.org/10.1016/j.measurement.2018.02.016.

[18] Vijayakumar K., Prabhaharan G., Asokan P., et al. (2003) Optimization of multi-pass turning operations using ant colony system. International Journal of Machine Tools & Manufacture 43(15):1633-1639. https://doi.org/10.1016/S0890-6955(03)00081-6.

[19] Qu S., Zhao J., Wang T. (2017) Experimental study and machining parameter optimization in milling thin-walled plates based on NSGA-II. Int J Adv Manuf Technol 89:2399–2409. https://doi.org/10.1007/s00170-016-9265-1.

[20] Sreeram S., Kumar A. S., Rahman M., et al. (2006) Optimization of cutting parameters in micro end milling operations in dry cutting condition using genetic algorithms. Int J Adv Manuf Technol 30(11-12):1030-1039. https://doi.org/ 10.1007/s00170-005-0148-0.

[21] Kumar A., Majumder H., Vivekananda K., et al. (2017) NSGA-II approach for multi-objective optimization of wire electrical discharge machining process parameter on Inconel 718. Materials

Today: Proceedings 4(2): 2194-2202.

[22] Wu M., Wang W., Shi D., et al. (2021) Improved box-counting methods to directly estimate the fractal dimension of a rough surface. Measurement 177: 109303. https://doi.org/10.1016/j.measurement. 2021.109303.

[23] Bai Q., Yang K., Liang Y., et al. (2009) Tool runout effects on wear and mechanics behavior in microend milling. J. Vac. Sci. Technol. B, 27(3): 1566-1572. https://doi.org/10.1116/1.3058729

[24] Bai Q., Li K., Liang Y., et al. (2015) Wear and breakage behaviors of PCD small-diameter endmill: a case study on machining 2A12 aluminum alloy. Int J Adv Manuf Technol 77(5-8):839-846. https: //doi.org/10.1007/s00170-014-6435-x.

[25] Jing C., Tang W. (2016) Ga-doped ZnO thin film surface characterization by wavelet and fractal analysis. Applied Surface Science 364:843-849. https://doi.org/10.1016/j.apsusc.2015.12.234

[26] Wang F., Cheng X., Zheng G.M., et al. (2019) Study of micromilling parameters and processes for thin wall fabrications. Precision Engineering 56:246-254. https://doi.org/10.1016/j.precisioneng.2018.12.005.